Dynamical processes on Random Geometric Graphs

Fabian Ying

September, 2013

Last updated: September 29, 2013

1 Introduction

We are interested in studying dynamical processes on spatially embedded graphs and in particular the effect of spatial embeddedness on the dynamics. To our knowledge, only a few dynamical processes on spatial networks have been studied [8]. We considered Random geometric graphs (RGG), a spatially embedded network and studied the Watts' model [5] (in particular the equilibrium fraction of infected nodes ρ) and the classical Voter model (in particular the consensus time T) on these graphs.

2 Random geometric graphs

Random geometric graphs (RGG) are random graphs on a bounded region (e.g. $[0,1]^d$ or $[0,1)^d$) generated by placing vertices (or nodes - we will be using both terms interchangeably) uniformly at random on the region and connecting nodes if their distance is less than some fixed r, called the distance parameter. We considered the RGGs on the unit-hypercube $[0,1]^d$ and on the unit-hypertorus $[0,1)^d$ where d is the dimension of the embedding space. The two regions differ in that the latter region allows edges through the boundary (*periodic boundary condition*) whereas the former does not (*open boundary condition*). Figure 1 (a) shows one realization of a RGG on the unit-squre $[0,1]^2$ and Figure 1 (b) illustrates the difference between the two boundary conditions with the red edges being the additional edges added on the two-dimensional torus $[0,1)^2$. In the following sections RGGs on $[0,1]^d$ and $[0,1)^d$ will be called *non-toroidal* and *toroidal*, respectively. We will see that the boundary conditions will have a non-trivial effect on the dynamics.

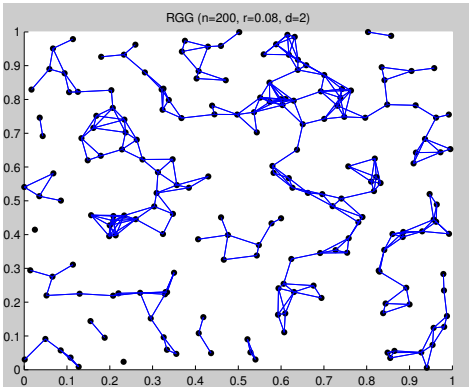

(a) non-toroidal RGG with 200 vertices and $r = 0.08$ in 2 dimensions

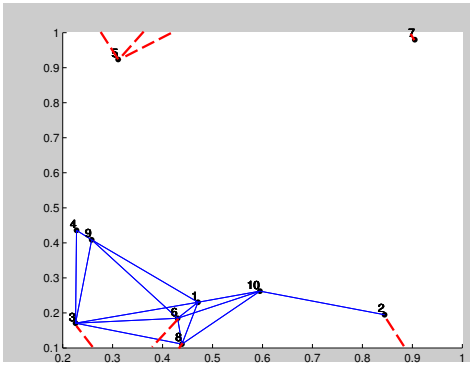

(b) RGG with 15 nodes. The red dashed edges are added for periodic boundary conditions

Figure 1: Toroidal and non-toroidal RGGs

3 Watts' model

We studied the Watts' cascade model on both types of RGGs [5] with uniform threshold $\phi = 0.18$, as in the original Watts' paper. The system size n is 1000 which is considerably small. These two values ϕ and n are fixed for the remainder of the section. The value of interest is the fraction of infected (or active) nodes ρ at the time when the graph has reached equilibrium (i.e. the state at which no more vertices become infected). We numerically evaluate ρ while varying the distance parameter r. Most results have been averaged over 100 realizations for accuracy.

3.1 Initial findings

For different sizes of initial seed fraction ρ_0, we see a qualitative difference between $\rho_0 > \phi$ and $\rho_0 < \phi$. In Figure 2, we plotted ρ vs r for both $\rho_0 > \phi$ (Fig. 2 (a)) and $\rho_0 < \phi$ (Fig. 2 (b)) and in each case for both toroidal (green line) and non-toroidal RGGs (blue line). In the former case, we see only one transition of ρ from ρ_0 to 1 as r increases while in the latter case there is a second transition from ρ to 1. The existence of the second transition can be trivially explained as with increasing r, the mean degree z increases and for sufficiently high z (or r), vertices have a fraction of infected neighbors of approximately $\rho_0 < \phi$, hence most vertices do not become infected and the equilibrium state is immediately reached. In the former case however for large r, most vertices become infected in the first time step as $\rho_0 > \phi$ and we reach again almost instant equilibrium but this time with $\rho = 1$.

3.2 Mean-field theories

We applied the p_k- and $P(k, k')$-theories [1, 2] on both types of random geometric graphs and plotted the result in Figure 3 for $\rho_0 > \phi$ and $\rho_0 < \phi$. The green dashed line shows the p_k-theory prediction and the red solid line shows the $P(k, k')$-theory prediction. We see that both mean-field theories predict the trend very well, but lack of accuracy. This result is not surprising since RGGs are generally highly clustered, so we don't expect mean-field theories to be accurate as they assume locally tree-like structure, although they do sometimes show high accuracy on clustered graphs [3]. Gleeson also pointed out that the lack of accuracy may also be due to the small size effect.

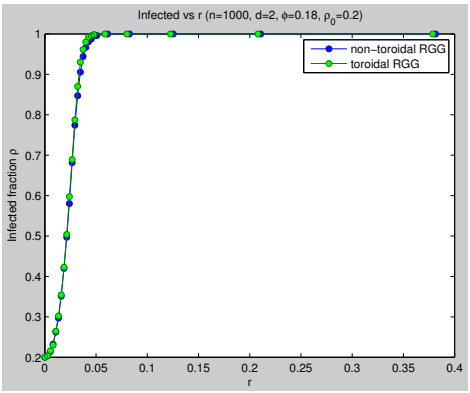

(a) $\rho_0 = 0.2 > \phi$

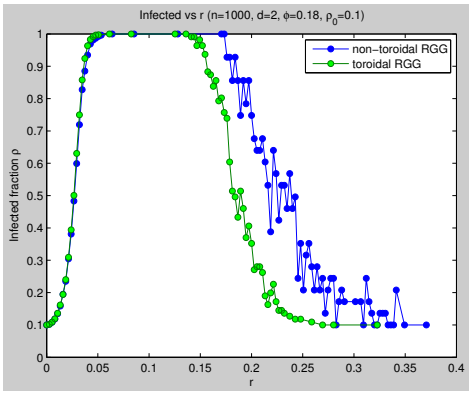

(b) $\rho_0 = 0.1 < \phi$

Figure 2: Watts' model on RGG

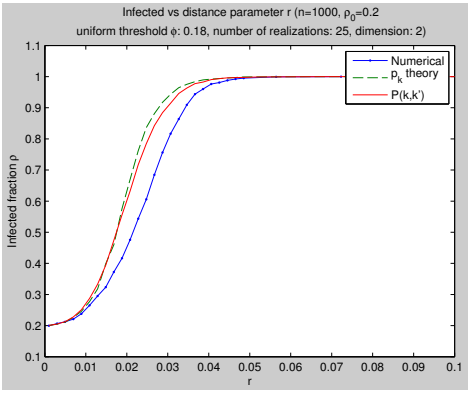

(a) $\rho_0 = 0.2 > \phi$

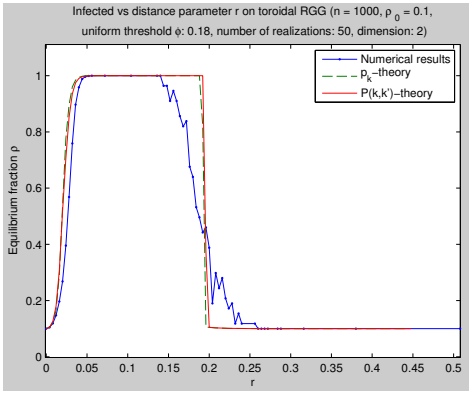

(b) $\rho_0 = 0.1 < \phi$

Figure 3: p_k- and $P(k, k')$-theories on non-toroidal RGGs

3.3 Increasing dimensions

We now study the effect of increasing the dimension of the embedding space. In Figure 4, we plotted the infected fraction ρ with $rho_0 = 0.2$ for dimensions $d = 2 - 15$ on non-toroidal (left figure) and toroidal RGGs (right figure). We first notice that toroidal RGGs in higher dimensions experience the transition at lower r, indicating the in higher dimensions more edges are added through the boundary, hence we reach the same mean degree z at lower r.

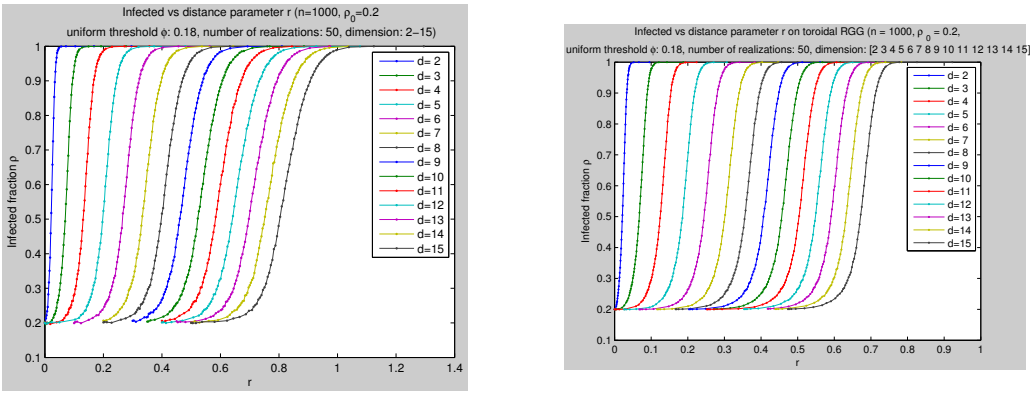

(a) non-toroidal RGG

(b) toroidal RGG

Figure 4: Infected fraction ρ for dimension $d = 2 - 15$ on non-toroidal (left) and toroidal RGGs (right)

We also notice a scaling behaviour for both types of graphs. The graphs suggest a scaling by $\frac{r-R(d)}{c(d)}$ where $R(d)$ and $c(d)$ is a function of d (and technically also of n, ϕ, ρ_0) and represent the transition shift and transition length respectively (see Figure 5 for illustration). Figure 6 shows the collapsed scal-

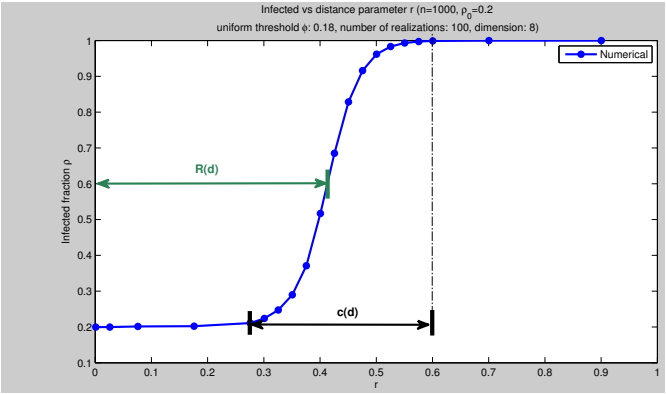

Figure 5: Illustration of $R(d)$ and $c(d)$

ing function for both type of RGG using the above scaling and we see a great collapse. In Figure 7, we plotted the numerical values of $R(d)$ and $c(d)$ and see that $R(d) \sim O(\sqrt{d})$ and $c(d)$ saturates to a constant value. So far no analytical approach has been found to deduce these scaling values. It has been suggested that renomalization techniques can be applied.

3.4 Comparison to Erdös-Renyi Graphs

We also compared the behaviour of the dynamic on RGGs to Erdös-Renyi Graphs (ER-Graph). Many structural properties of toroidal RGGs are similar to ER-Graph in the limiting case of $d \to \infty$, e.g. critical connectivity in the percolation theory [4] or the degree distribution p_k (for any dimension d). In Fig. 8, we plotted infected fraction ρ against the mean degree z for non-toroidal RGG (left) and toroidal RGG (right) for dimensions 2, 5, 10, 50 and 100. We also plotted the ρ for ER-Graph (black dashed line). We can see that for the system size of $n = 1000$, the toroidal RGG shows a behaviour approximate to the ER-Graph in higher dimensions, whereas non-toroidal

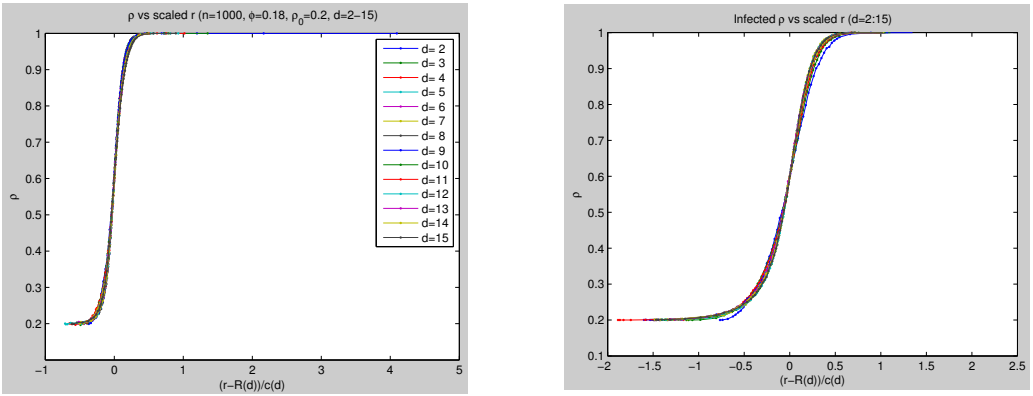

(a) non-toroidal RGG

(b) toroidal RGG

Figure 6: Scaling plot

RGGs diverges in higher dimensions. This indicates that the boundary condition plays a significant part in the dynamics and in higher dimensions more edges are added in toroidal RGGs which affect the dynamics.

3.5 Largest connected component

Next, we studied the largest connected component size and compared this value to the infected fraction ρ. In Fig. 9, we plotted ρ and the larg. connected comp. size in the same graph for $\rho = 0.2$ and $\rho_0 = 0.01$ and notice a strong correlation. Especially for low ρ_0, we see an accurate match between the largest component size, suggesting that in most cases the largest connected component is fully infected and makes up most of the infected nodes. This is supported by Fig. 10 which shows the infected fraction for $\phi = 0$,

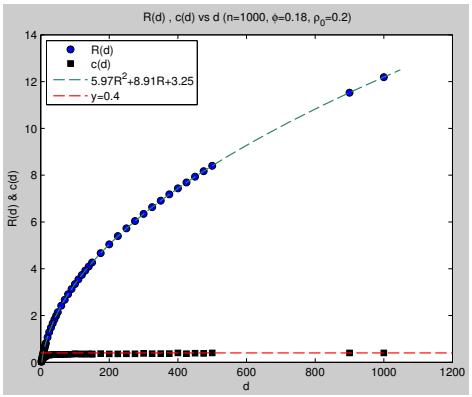

(a) non-toroidal RGG

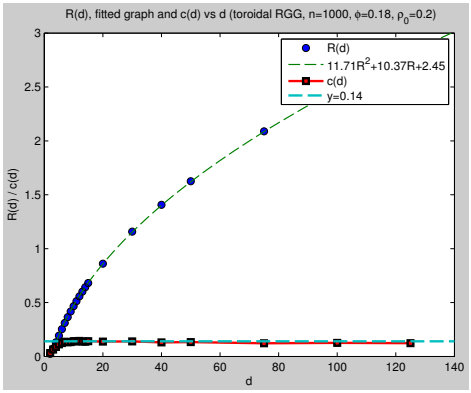

(b) toroidal RGG

Figure 7: Scaling values. Numerical values for $R(d)$ and $c(d)$ and fitted graph for $R(d)$

i.e. in the case when a component becomes fully infected with a single seed node, since the graph in Fig. 10 is identical to the one in Fig. 9(b). There is a intuitive explanation for this, since the transition connectivity (or critical connectivity) α_c is typically less than 5 and with our choice of $\phi = 0.18$ in the simulations, a single seed node will infect most of its neighbors as their degree is typically less than 5 and thereafter infect the whole component. In most cases, we will have a small seed node in the largest connected component (or at least it averages like that). Hence our choice of ϕ and the homogeneity of the degree distribution causes the strong correlation between largest connected component size and infected fraction. One thing we need to node is that the Watts' model on spatial networks lack self-averaging, so

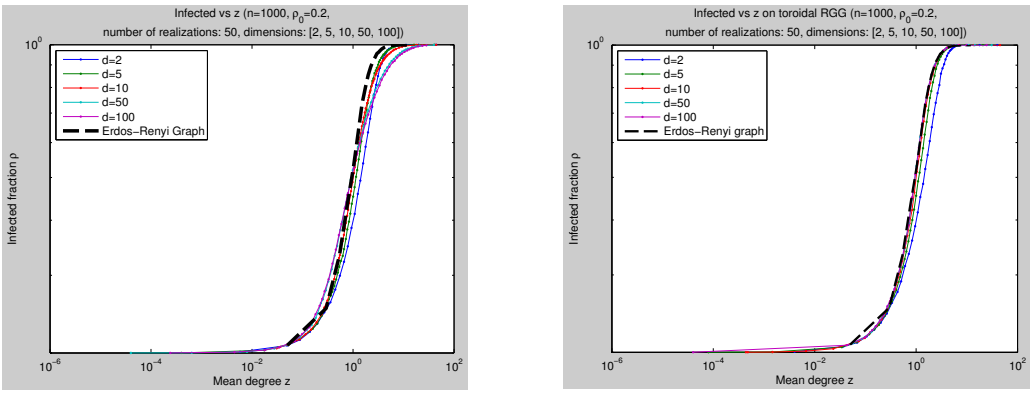

(a) non-toroidal RGG

(b) toroidal RGG

Figure 8: Infected fraction ρ vs mean degree z. We see that toroidal RGG approach the behaviour of Erdös-Renyi graph in higher dimensions whereas non-toroidal do not.

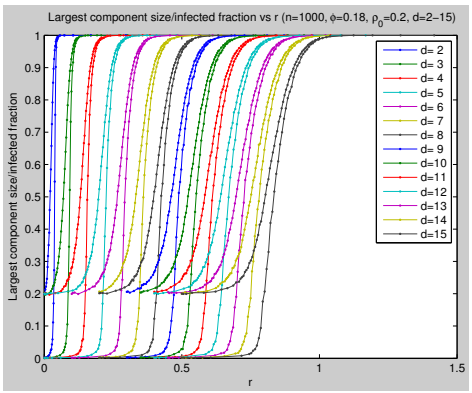

(a) $\rho_0 = 0.2$

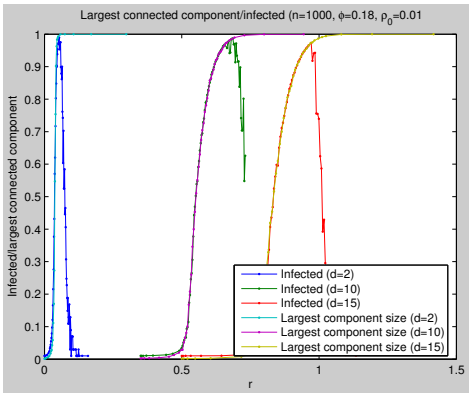

(b) $\rho_0 = 0.01$

Figure 9: Largest connected component size and infected fraction ρ. (a) We see that the largest component size approaches ρ at the end of the transition for all dimensions for $\rho_0 = 0.2$ (b) With smaller seed size of $\rho_0 = 0.01$ we see a perfect match for the transition. *(see text for explanation)*

this needs to be confirmed. [9]

3.6 Summary

In summary, we have studied the infected fraction ρ of nodes at equilibrium state on RGGs, using the Watts' model with $\phi = 0.18$ and showed a strong correlation between largest connected component size and ρ. We also observed a dimensional scaling behaviour of the form $\frac{r-R(d)}{c(d)}$ and numerically showed that $R(d) \sim O(\sqrt{d})$ and $c(d)$ saturates at constant value. We showed that toroidal RGGs reflect the behaviour of ER-Graphs in higher dimensions

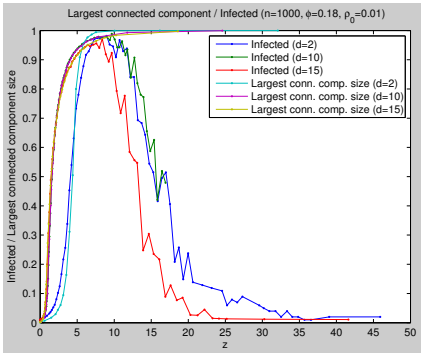

Figure 10: Largest connected component size and infected fraction ρ vs mean degree z. We see that the critical connectivity is typically less than 5

while non-toroidal do not. Lastly, we observed that the mean-field p_k and $P(k, k')$-theories do not give a good prediction for RGGs.

4 Voter model

The second model we studied is the classical Voter model as defined in [6] Section II. It is a binary state model with the following updating rule (at each time step dt:

1. Pick a random node (a voter)

2. The voter adopts the sate of a random neighbor

In this section, we use a system size of 300 unless otherwise stated and look at the consensus time T, the time at which all connected components reached consensus (i.e. the same state). Note the difference to *global consensus* which requires that *all nodes* have the same state, not just that each component

has the same states. Also we set $\rho = 0.5$, i.e. there are initially equal number of nodes at either state.

4.1 Initial findings

In Fig. 11, we plotted the consensus T against the distance parameter r for RGG. We see three phases as r increases: First an instant consensus, secondly we observe a peak in consensus time and lastly a saturation to a fast, but not instant consensus. Fig. 12 shows the largest connected component size and the variance of the non-giant cluster/component sizes against r together with the consensus time T. We see that the consensus time peaks near the critical connectivity α_c, i.e. near the point when a large connected component emerges. This can be explained by high variance of non-giant cluster sizes near α_c, indicating diverse cluster sizes which lead to the observed phenomenon called *critical slowing down*. Intuitively, we can also say that the largest connected component is approximately a 1-D lattice, so it simulates a random walk on a 1-D lattice which has very high absorption time. We also notice that the saturation occurs for all $r > r_c + \delta$ for some $\delta > 0$, even for maximal $r = \sqrt{(}d)$. Therefore we numerically see that in the third phase, a RGG behaves the same as a fully connected graph. In [6], Sood *et al* showed for a fully connected graph that

$$T(\rho) = n\left[(1-\rho)\ln\frac{1}{1-\rho} + \rho\ln\frac{1}{\rho}\right] \tag{1}$$

where ρ is fraction of nodes initially set to state 0 (or 1) and n is the system size.

In particular, we see for fixed ρ, the consensus time T scales with n, therefore

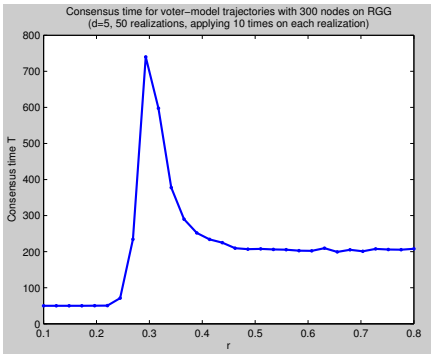

Figure 11: Consensus time T vs. r, averaged over 50 realization

RGGs in the third phase show the same scaling behaviour as d-dimensional lattices for $d > 2$ [7]. Also for $\rho = 0.5$, $T(\rho) = n \ln 2$, as we can see confirmed in Fig. 13 which shows the consensus time T for different system sizes n at $r = 0.3$. Noteworthy is the last point for $n = 2000$ which seems to diverge from the predicted value. This will need to be more closely studied as

4.2 Summary

In summary, we showed for small n numerically three 'phases' of consensus time:

1. $r < r_c$: Instant consensus due to very low cluster sizes
2. $r \approx r_c$: 'Critical slowing down' with very high consensus time since we have very diverse range of cluster sizes
3. $r >> r_c$ RGG enters a regime that shows the same behaviour as a fully connected graph.

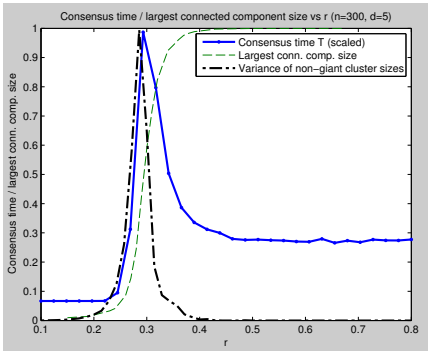

Figure 12: Consensus time T, largest connected component size and variance of non-giant component sizes vs. r. We observe a *critical slowing down* near the critical point

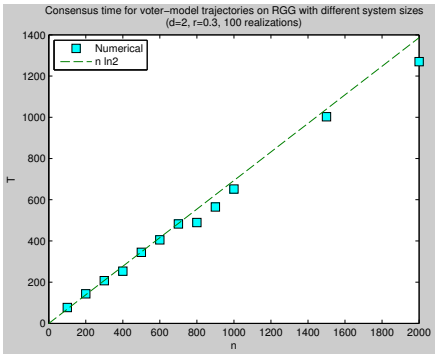

Figure 13: Consensus time T vs system size n

5 Future work

With these results there are a vast possibilities of future work in both of the models.

5.1 Watts' model

Due to the nature of question, there are many variables (e.g. n, ϕ, d, ρ_0, r) and we have only explored the effect of r, d and to some extent ρ_0. Hence it is natural to consider varying ϕ, especially as we saw in Section 3.5, that our particular choice of $\phi = 0.18$ caused that a single initial seed node will typically infect the whole component, so one may use in future a higher ϕ and possibly observe a critical ϕ_c at which the behaviour changes qualitatively. A larger system size n (while fixing the mean degree z) will likely reduce the boundary effect and possibly give better approximation of the mean-field theories (p_k and $P(k, k')$. We may also consider to study the existence of a finite-size scaling. In Section 3.3, we observed a scaling behaviour and one may try to formulate an analytical derivation for the function $R(d)$ and $c(d)$. Lastly, as we only considered the case for $\phi < \rho_0$ with only one transition, we may also study the second transition for $\phi > \rho_0$. We expect a strong dependence on ρ_0 as it is the case for Erdös-Renyi graphs [1].

5.2 Voter model

The boundary effect of the voter model has not been studied, neither has the effect of increasing the dimension of the space which are interesting things to study in future.

5.3 RGG

Another thing we can consider in future is to have variations of random geometric graphs with a region different than unit-cube and unit-torus or with nodes connected to each other non-deterministic, e.g. with probability proportional to $\frac{1}{r}$. This will allow a small number of long-range links which might change the dynamics.

References

[1] J. P. Gleeson and D. J. Cahalane: *Seed size strongly affects cascades on random networks*, Phys. Rev. E **75**, 056103 (2007)

[2] J. P. Gleeson: *Cascades on correlated and modular random networks*, Phys. Rev. E **77**, 046117 (2008)

[3] S. Melnik et al: *The unreasonable effectiveness of tree-based theory for networks with clustering*, Phys. Rev. E **83**, 036112 (2011)

[4] J. Dall and M. Chfristensen: *Random geometric graphs*, Phys. Rev. E **66**, 016121 (2002)

[5] D. J. Watts: *A simple model of global cascades on random networks*, Proc. Natl. Aca. Sci. U.S.A **92**, 5766 (2002)

[6] V. Sood et al: *Voter models on heterogeneous networks*, Phy. rev. E **77**, 041121 (2008)

[7] P. L. Krapisvky: *Kinetics of monomer-monomer surface catalytic reactions*, Phys. Rev. A **45** 1067 (1992)

[8] M. Barthélemy *Spatial networks*, Phys. Rep. **499** (2011)

[9] A. Asztalos et al: *Cascading failures in spatially-embedded random networks*, arXiv:1309.2175 [physics.soc-ph] (2013)